Nanoscale

PAPER

View Article Online
View Journal | View Issue

Open Access Article. Published on 28 noiembrie 2018. Downloaded on 14.02.2026 15:02:16.
This article is licensed under a Creative Commons Attribution 3.0 Unported Licence.

Check for updates

Cite this: *Nanoscale*, 2018, **10**, 22792

3D characterization of heat-induced morphological changes of Au nanostars by fast *in situ* electron tomography†

Hans Vanrompay,‡[a] Eva Bladt,‡[a] Wiebke Albrecht,‡[a] Armand Béché,[a] Marina Zakhozheva,[b] Ana Sánchez-Iglesias,[c] Luis M. Liz-Marzán[c,d] and Sara Bals *[a]

Received 16th October 2018,
Accepted 28th November 2018

DOI: 10.1039/c8nr08376b

rsc.li/nanoscale

A thorough understanding of the thermal stability and potential reshaping of anisotropic gold nanostars is required for various potential applications. Combination of a tomographic heating holder with fast tilt series acquisition has been used to monitor temperature-induced morphological changes of Au nanostars. The outcome of our 3D investigations can be used as an input for boundary element method simulations, enabling us to investigate the influence of reshaping on the nanostars' plasmonic properties. Our work leads to a better understanding of the mechanism behind thermal reshaping. In addition, the approach presented here is generic and can hence be applied to a wide variety of nanoparticles made of different materials and with arbitrary morphology.

Introduction

Gold nanoparticles (Au NPs) have shown enormous potential for applications in various fields, ranging from biology and medicine to chemistry and physics. Next to their catalytic activity, high chemical stability and bio-compatibility, Au NPs exhibit intriguing optical properties due to well-defined localized surface plasmon resonances (LSPRs).[1,2] Such LSPRs lead to strong absorption and scattering of light, which causes a significant enhancement of incoming electromagnetic fields at the nanoparticles' surface.[3,4] The plasmonic properties of Au NPs can be tuned by varying their morphology, surface charge or dielectric environment.[1,2,5]

As compared to spherical Au NPs, anisotropic NPs show superior plasmonic properties, with electromagnetic field enhancements that are orders of magnitude larger.[6,7] Branched NPs with sharp tips, known as nanostars (NSs), have therefore gained significant attention during the last decade,[8–10] as they form ideal substrates for *e.g.* surface-enhanced Raman scattering (SERS),[11,12] or generation of hot electrons.[12–15] Moreover, by tailoring the NP morphology, the corresponding plasmon resonances can be conveniently tuned and shifted into the NIR wavelength range, thereby enabling applications in biological environments.[9,10] In fact, due to their efficient light-to-heat conversion, Au NSs have been employed for both *in vitro* and *in vivo* studies of photothermal cancer therapy.[8] The conversion efficiency strongly depends on the spectral position and intensity of the plasmon resonance. Therefore, it is essential to preserve the morphology of Au NSs, and thus their LSPR response upon laser excitation.[16,17] Unfortunately, previous studies have shown that anisotropic Au NPs readily deform into more rounded morphologies, upon heating or laser excitation.[16–18] For example, Au nanorods reshape at temperatures that are hundreds of degrees below the bulk melting point of gold.[19] In applications where Au NPs are subjected to intense laser irradiation, such elevated temperatures can easily be reached, especially if pulsed lasers are used.[20–22] Obviously, such heat-induced deformations will affect the optical properties of the Au NPs and consequently limit those applications where the morphology needs to be preserved. However, we do not possess sufficient information yet on the heat-induced morphological evolution of highly anisotropic Au NPs and the correlated change of their optical properties.

Up to date, most studies have focused on understanding the (photo)thermal stability of large ensembles of Au NPs, *e.g.* monitoring the extinction spectrum as a function of temperature.[19,23,24] On the other hand, *in situ* heating experiments in a

[a]*Electron Microscopy for Materials Science (EMAT), University of Antwerp, Groenenborgerlaan 171, 2020 Antwerp, Belgium. E-mail: sara.bals@uantwerpen.be*
[b]*DENSsolutions, Informaticalaan 12, 2628ZD Delft, The Netherlands*
[c]*Bionanoplasmonics Laboratory, CIC biomaGUNE, Paseo de Miramón 182, 20014 Donostia - San Sebastian, Spain*
[d]*Ikerbasque, Basque Foundation for Science, 48011 Bilbao, Spain*

†Electronic supplementary information (ESI) available. See DOI: 10.1039/c8nr08376b

‡These authors contributed equally.

This journal is © The Royal Society of Chemistry 2018

Open Access Article. Published on 28 noiembrie 2018. Downloaded on 14.02.2026 15:02:16.
This article is licensed under a Creative Commons Attribution 3.0 Unported Licence.

transmission electron microscope (TEM) may enable the direct observation of temperature-induced changes in single particles. However, so far, these studies have been consistently based on conventional, two-dimensional (2D) images, which inherently limit such investigations to simple geometries such as rods or spheres.[19,25,26] To monitor the deformation of more complicated anisotropic structures like (irregular) Au NSs, 2D projection images are insufficient. Electron tomography is currently a standard technique to visualize the morphology and internal structure of a wide variety of nanostructures in three dimensions (3D). The approach is based on the acquisition of a series of 2D projection images collected at different tilt angles over an angular range that is as large as possible. Due to practical limitations however, the tilt range is typically limited to ±80°.[27] Exciting new developments in the field of TEM holder fabrication, have recently resulted in heating holders that reach the tilt range required for electron tomography, thereby allowing for novel *in situ* 3D heating studies.

However, to perform elaborate *in situ* heating experiments in 3D, several important limitations need to be overcome. A major drawback of electron tomography is the time needed to acquire a full tomographic tilt series, which will hamper the investigation of fast processes in 3D.[28] In addition, long exposure times may cause undesired changes within the NPs, making it difficult to differentiate between heat-induced and electron beam induced changes. Therefore, one of the emerging challenges in the field of electron tomography is to improve the speed of tomography experiments, while preserving the quality of the 3D reconstructions. If this challenge can be overcome, it will become possible to study processes *in situ*, in 3D. Such experiments cannot be easily performed using conventional electron tomography due to possible beam-induced changes or simply time limitations.

We therefore propose a novel acquisition approach where a tilt series of 2D high angle annular dark field scanning transmission electron microscopy (HAADF-STEM) projection images is acquired within a few minutes. By continuously tilting the holder and simultaneously acquiring projection images while focusing and tracking the particle, we were able to reduce the total acquisition time for a tilt series by a factor of ten. In this manner, we were able to study the 3D morphological evolution of single Au NSs as a function of both heating time and temperature. Experiments were performed at 200 °C, 300 °C and 400 °C for a total heating time of 20 minutes, in order to decouple the effect of temperature and total amount of delivered heat on the morphological changes. By using the measured 3D shape as an input for boundary element method (BEM) simulations, we determined the connection between the 3D shape transformations and the consequent changes of the optical properties at elevated temperatures. This information is highly valuable toward understanding Au NSs' performance in practical applications. Fast HAADF-STEM tomography furthermore paves the way towards a wide variety of 3D *in situ* studies.

Results and discussion

Au NSs were obtained through a seed-mediated growth process, in the presence of cetyltrimethylammonium bromide (CTAB). In Fig. S1,† a HAADF-STEM overview image of the sample is presented. From projection images, such as those in Fig. S1b and c,† it is clear that the NPs exhibit an anisotropic shape with several branches, apparently in random orientations. To retrieve the 3D structure of a NS, a conventional tilt series of images was recorded for a single NS, shown in Fig. 1a. Hereby, the sample was tilted from −74° to +74°, with a tilt increment of 3°. For each tilt angle, the NS was shifted back to the middle of the field of view and the image was refocused before the next acquisition. In this manner, the necessary time to acquire images over a tilt range of ±74° was approximately 1 hour. After the acquisition, the images were aligned with respect to each other using a phase correlation procedure.[29–32] The outcome was used as an input for the ASTRA toolbox[33] implementation of the Expectation-Maximization algorithm (EM),[34] resulting in a 3D reconstruction of the morphology of the NS. A 3D visualization is presented in Fig. 1b, where the highly anisotropic and somehow irregular shape of the particle is obvious. Next, we acquired a tilt series of the same NP in a continuous manner, meaning that the holder was rotating uninterruptedly and intermediate refocusing and repositioning was performed manually while tilting. During the fast acquisition, the holder was continuously tilted and approximately 360 2D projection images over

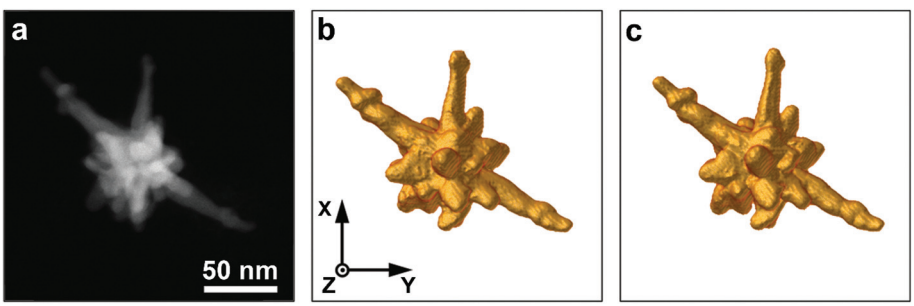

Fig. 1 (a) 2D HAADF-STEM image of an Au NS. (b, c) 3D visualizations of the outcome of the conventional tomography experiment (b) and the fast tomography experiment (c).

Open Access Article. Published on 28 noiembrie 2018. Downloaded on 14.02.2026 15:02:16.
This article is licensed under a Creative Commons Attribution 3.0 Unported Licence.

an angular range of ±74° were acquired. This corresponds to a tilt increment of 0.41° per image. Images with a size of 1024 × 1024 and a frame time of 1 s were acquired, resulting in a total acquisition time of approximately 6 minutes. The continuous tilting speed of the holder, resulting in the 6 min acquisition time, was hereby chosen to ensure a good ratio between speed and quality of the single images. Furthermore, it is necessary to keep the tilt angle difference per image small enough to treat the images as static projections. Projection images that were heavily affected by blurring or motion effects were afterwards excluded.

Such effects were unavoidable due to the fast acquisition, but removal of these images from the tilt series is not problematic, given the oversampling of projection images compared to a conventional series (*ca.* 50 images). Further post-processing of the remaining stack of images improved the quality of the individual projection images. Next, the tilt series was aligned and served as an input for the tomography reconstruction. Further technical details on the acquisition, post-processing, alignment and reconstruction are provided in the ESI.† The resulting 3D reconstruction is displayed in Fig. 1c, showing excellent visual agreement with the conventional reconstruction (Fig. 1b). The agreement is further confirmed by calculating the difference between both reconstructions. Details and discussion on the calculation of the difference reconstruction are provided in the ESI.† As a result, we can conclude that the fast tomography approach results in an accurate 3D representation of the investigated nanostructure.

The drastic reduction in acquisition time enables the investigation of the morphology of nanomaterials in 3D while heating, with a higher sampling rate compared to conventional tomography. Such experiments have been performed in 2D, but 3D results were not available so far. Fast acquisition has the additional advantage that the electron dose and dose rate can be reduced. Dose reduction is crucial, since it was recently shown that even apparently beam-insensitive nanomaterials such as Au nanorods exhibit an altered thermal stability upon *in situ* heating, compared to *ex situ* experiments.[35] In what follows, we make use of this novel technique to study the heat-induced 3D morphological changes of highly anisotropic Au NSs. Aided by the drastic reduction in acquisition time of the fast tomography experiment, gradual changes can be examined, as opposed to earlier *ex situ* work in which electron tomography series could only be obtained before and after heating.[36] Monitoring these changes on the same NS will not only give us insight into the thermal stability of these NSs but will also reveal local structural differences and their influence on the heat-induced reshaping. The latter cannot be revealed by other indirect techniques such as optical ensemble measurements. Yet, such information is crucial to understand the NSs instability and reshaping behavior at elevated temperatures. Based on previous studies,[16,19,20,22] we chose heating temperatures of 200 °C, 300 °C and 400 °C, and a total heating time of 20 min for each temperature. Below 200 °C, morphological changes occur slowly, on the order of hours, whereas above 400 °C reshaping of Au NPs is almost instantaneous.[16,19,20] To determine the 3D morphological evolution as a function of time, fast tilt series were acquired at intermediate time steps of 30 s, 60 s, 90 s, 120 s, 180 s, 300 s, 600 s and 1200 s for each temperature. Hence, the particle was heated for the given time and subsequently cooled down to room temperature, so as to quench further heat-induced morphological transformations. After quenching, a fast tomographic series was acquired. This procedure was repeated for the various selected time steps. In this manner, the sampling of the morphological evolution is only limited by the number of acquired tilt series, which is greatly enhanced with our fast acquisition approach.

A complete time series of the morphological evolution of an Au NS is shown in Fig. 2, for the temperature of 200 °C. It is clear that all branches of the Au NS deform upon heating. Indeed, as indicated by the black arrows, a transformation was observed from relatively long and thin branches into short but broader branches, similar to the thermally induced deformation observed in 2D TEM images for other Au NPs with symmetric geometries.[16,17,19] Most of the reshaping occurs during the first time steps of 30 s and 60 s (Fig. 2b and c). After 60 s (Fig. 2d–i), only minor additional morphological changes were observed. Based on these qualitative findings and the fact that reshaping gets enhanced at higher temperatures, we assume faster reshaping at 400 °C. Therefore, we acquired additional time series at 10 s and 20 s for 400 °C. The 3D visualizations of the complete time series for 300 °C and 400 °C are presented in the ESI† (Fig. S5 and S6,† respectively).

To study the effect of temperature on the morphology of Au NS, we compared the morphological changes at 30 s and 1200 s, for heating at 200 °C, 300 °C and 400 °C, as illustrated in Fig. 3. At the higher temperatures, a similar morphological evolution can be noticed as discussed above. For all temperatures, most of the deformation takes place within the first 30 s, after which the deformation slows down. However, the amount of total reshaping increases with increasing temperature and the observed final shape after heating for 1200 s strongly depends on the applied temperature. Whereas blunt tips can still be observed after 1200 s at 200 °C, no tip-like features can be observed at 400 °C, even after 30 s. Therefore, we conclude that in the time range presently investigated, the heating temperature has a more dominant influence than the duration of heating, which is in agreement with indirect optical bulk measurements.[19]

To quantitatively analyze the morphological evolution as a function of local structural features, we calculated the differences between successive reconstructions. Details on difference calculations are provided in the ESI.† Fig. 4 displays the local volume redistribution for the first two heating steps (Fig. 4a, b, d, e and g, h) and the last heating step (Fig. 4c, f and i) for each temperature. Local volume increments and reductions are presented as green and red regions, respectively. It is immediately obvious that, in regions with a higher curvature, and thus predominantly at the tips of the branches, the local volume decreases whereas local volume increments were identified at low curvature areas. Furthermore, as hypothesized above, we quantitatively show that volume redistribu-

 This journal is © The Royal Society of Chemistry 2018

Open Access Article. Published on 28 noiembrie 2018. Downloaded on 14.02.2026 15:02:16.
This article is licensed under a Creative Commons Attribution 3.0 Unported Licence.

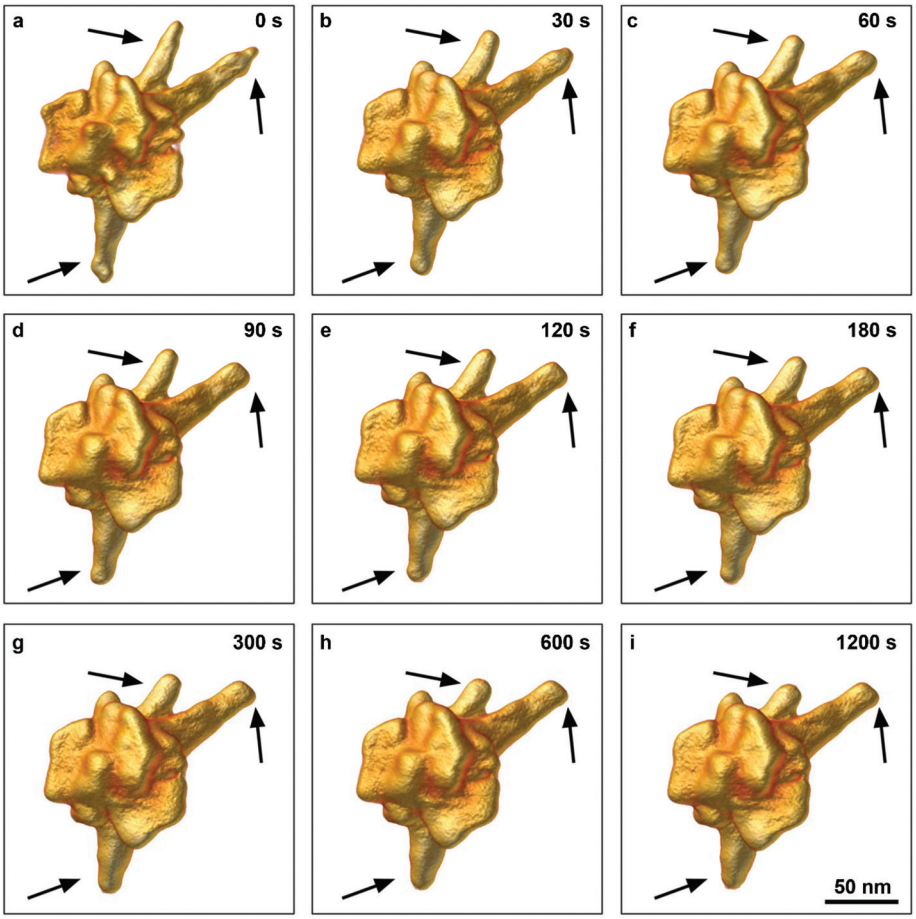

Fig. 2 (a–i) 3D visualizations of the same Au NS after different heating times at 200 °C. The black arrows point towards the regions where morphological changes can be clearly seen.

tions slow down for longer heating times. Additionally, a clear distinction can be seen for the different temperatures, as qualitatively discussed above. The higher the temperature, the farther the atoms can diffuse. After 30 s at 200 °C, only the tips of the nanobranches disappear (red areas in Fig. 4a), the atoms getting redistributed on the sides of the same branches (green areas in Fig. 4a). At 300 °C, a large part of each branch is found to diffuse toward the body of the NS, and at 400 °C atoms from the branches completely redistribute toward the body of the NS. Thus, we unambiguously show that atoms diffuse from the sharpest parts of the nanobranches, or the NS tips, toward areas of lower curvature. A process that gets accelerated by increasing temperature, thereby confirming a previous study on simple geometries which was based on 2D projections.[16]

In order to quantitatively compare the effect of temperature and heating duration on the reshaping, the total amount of redistributed volume at each heating step was calculated for each temperature. Since the total redistributed volume is directly related to the relative volume initially present in the branches of the NS, and a different NS was studied at each temperature, the amount of redistributed volume was normalized by the total volume of the branches of the initial NS. The initial volume of the branches was determined by segmenting the 3D reconstruction of the NS and separating the core from the branches. The resulting total amount of redistributed volume as a function of heating time is plotted in Fig. 4j (black: 200 °C, blue: 300 °C and magenta: 400 °C). The error bars (2%) on these measurements are determined by the accuracy of the required segmentation step (see ESI† for details). The results confirm that most of the heat-induced morphological changes occur within the first minute of heating, regardless of temperature. The plot in Fig. 4k illustrates in more detail the volume redistribution occurring during the first minute, indicating that most of the morphological changes already occurred after 30 s. When heating the NSs further, the particles converge to a more stable configuration and less extensive heat-induced morphological changes take place (Fig. 4j). The data points for the different temperatures demonstrate quantitatively that the magnitude of the morphological changes is determined by the heating temperature. At 200 °C, only (20 ± 2)% of the volume is redistributed after 30 s of heating. However, for 300 °C and 400 °C, the total redistributed volume after 30 s equals (52 ± 2)% and (89 ± 2)%, respectively. At the end of the heating time of 1200 s, the total redis-

Open Access Article. Published on 28 noiembrie 2018. Downloaded on 14.02.2026 15:02:16.
This article is licensed under a Creative Commons Attribution 3.0 Unported Licence.

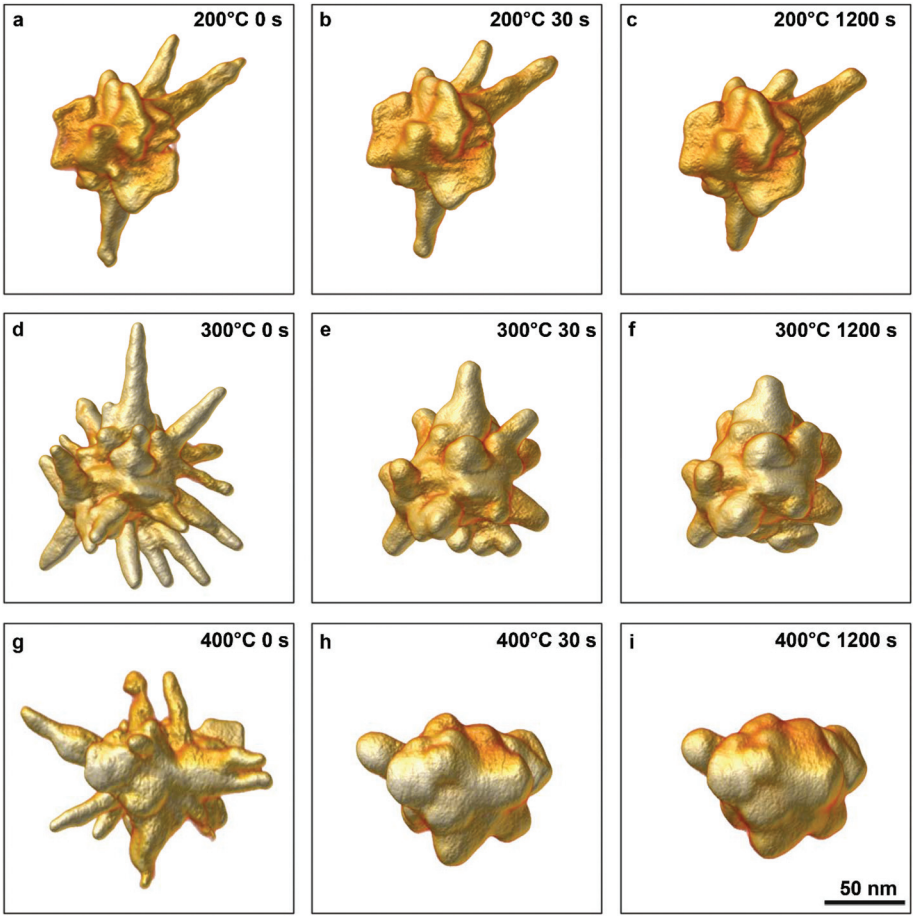

Fig. 3 3D visualizations, using fast tomography, of an Au NS before (a) and after heating for 30 s (b) and 1200 s (c) at 200 °C. 3D visualizations for the same time steps are shown for 300 °C (d–f) and 400 °C (g–i).

tributed volumes were (35 ± 2)%, (69 ± 2)% and (89 ± 2)%, for 200 °C, 300 °C and 400 °C, respectively. Thus, reshaping continues, though at a slower rate, after 30 s for 200 °C and 300 °C but does not progress further for 400 °C. Thus, the NS converges faster to its final morphology when a higher heating temperature is introduced. More specifically, at 400 °C no volume redistribution was observed after 20 s of heating, at which a plateau value was reached (Fig. 4k). Although most of the redistribution was completed within 30 s for 300 °C and 200 °C, reshaping continued up to about 300 s for 300 °C and for the total heating time of 1200 s for 200 °C.

Earlier thermal stability studies also found a clear dependence of the deformation of Au NPs on temperature.[16,19,20] For example, Petrova *et al.* compared the reshaping of Au nanorods at 100 °C, 150 °C, 200 °C and 250 °C, over the course of 1200 min, by optical ensemble extinction spectroscopy and scanning electron microscopy.[19] At 250 °C they observed complete reshaping of the Au NRs into a spherical shape, within about 20 min. For lower temperatures the final aspect ratio of 1 was not reached even after 1200 min, but intermediate aspect ratios were observed. The authors raised the questions whether these were real intermediate states or whether sample changes were then evolving very slowly. It should be mentioned that optical ensemble measurements can only give an average image due to sample polydispersity and possibly sintering of NPs. We are fully aware of the difference between heating in air or vacuum, nevertheless the results obtained here are of high interest to answer such questions, since they enable us to directly quantify changes for an individual NP in 3D. The results presented in Fig. 4 show that the amount of redistributed volume saturates over time, revealing that these are real intermediate states that do not change upon further heating at the same temperature. To fully comprehend the influence of the environment, these experiments will have to be extended to environmental TEM.

It is important to note that CTAB can be transformed by the electron beam into a protective amorphous carbon layer, which has been shown to prevent deformation of Au NRs upon *in situ* heating, even for heating at 400 °C for one hour.[35] This again stresses the need for a fast acquisition procedure to perform such *in situ* experiments in 3D. Over the course of time of one conventional tomography experiment, we were able to perform ten fast tomographic acquisitions. By continuously rotating while acquiring, we did not only lower the acqui-

 This journal is © The Royal Society of Chemistry 2018

Open Access Article. Published on 28 noiembrie 2018. Downloaded on 14.02.2026 15:02:16.
This article is licensed under a Creative Commons Attribution 3.0 Unported Licence.

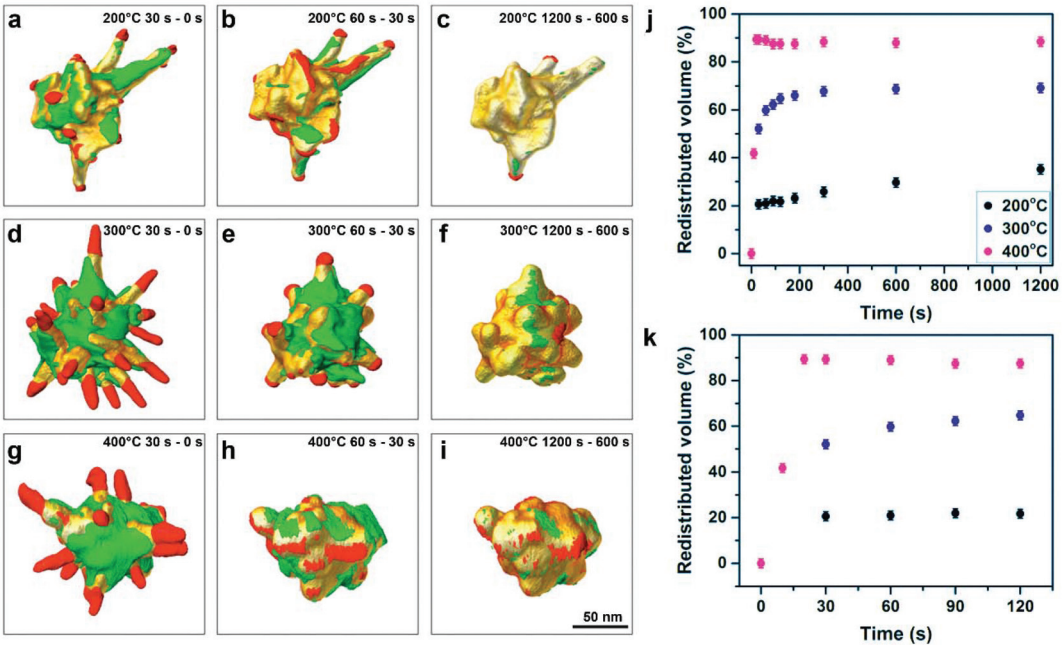

Fig. 4 (a–i) Visualizations of the morphological changes during two successive heating steps, where volume increments and volume reductions are depicted in green and red, respectively. The order of subtraction is indicated in each panel, together with the temperature of heating. (j) Total amount of redistributed volume normalized to the volume of the branches in the initial NS, as a function of time for 200 °C (black dots), 300 °C (blue dots) and 400 °C (magenta dots). (k) Detailed view of the volume redistribution occurring during the first two minutes.

sition time, but the electron dose rate was reduced as well. Consequently, the undesirable build-up of a surrounding carbon layer was limited during the initial acquisition and such a protective effect was minimized. However, we still observed a remaining small influence of a protective carbon layer, with respect to NSs that were out of the field of view during the experiment. For the case of heating at 400 °C for 1200 s, non-irradiated NSs exhibited a slightly more rounded morphology in comparison to the irradiated NSs (Fig. S7†). When heating at 300 °C for 1200 s, non-irradiated NSs showed a stronger deformation than the NS that was in the field of view. Nevertheless, branches could also still be observed for the non-irradiated NSs, similar to the NS in the field of view (Fig. S8†). Unfortunately, it is difficult to quantify the difference in deformation, as the specific initial morphology of NSs that were out of the field of view remains unknown.

It has been reported that the presence of sharp tips in both Pt NSs and Au NSs leads to a strong enhancement of the SERS activity.[9,10,37] The reshaping of sharp tips will therefore heavily influence the desired optical and electronic properties of NSs. Kumar *et al.* showed that the strong field enhancement of Au NSs was predominately directed by the angle and the sharpness of the tips.[9] In order to quantify the sharpness of the Au NS tips during the morphological evolution, the Gaussian curvature of the surface was calculated for every 3D reconstruction.[38] We demonstrate this calculation for the experiment performed at 300 °C, as the selected NS exhibited many branches.

The distributions of positive values of the tip curvature after 0 s, 30 s and 1200 s of heating at 300 °C are plotted in Fig. 5a. With increasing heating time, an overall increase in the relative occurrence of low curvature values, along with a decrease of high curvature values can be observed, thereby confirming the above observations. Specifically, the initial shoulder around 0.01 nm^{-2} (black histogram), indicated by the black arrow in the inset of Fig. 5a which can be attributed to the sharp tips, completely vanishes after heating for 30 s (green histogram). Accordingly, the relative frequencies around 0.003 nm^{-2} increase after 30 s, indicating the deformation toward blunter tips, *i.e.* more extended areas of lower curvature. After 1200 s (magenta histogram), no shoulders can be observed anymore, while the contributions around 0 nm^{-2} increase, due to the complete deformation of the tips. To visualize the curvature in 3D, Fig. 5b–d display the corresponding volume renderings for the Au NS before and after heating for 30 s and 1200 s at 300 °C, superimposed with a color map illustrating the measured Gaussian curvature for every nanobranch. The color scales linearly between −0.02 (blue) and 0.02 nm^{-2} (red). Overall, the curvature of the whole nanoparticle is distributed around 0 nm^{-2} (green), with contributions of high curvatures from the tips (red) and minimal contributions (blue) due to negative curvature where the tips grow out of the body of the NP. These visualizations confirm again the significant changes in curvature of the nanobranches upon heating. Once the NS has lost its most prominent features, the sharp tips of its branches, the morphological evolution slows down. This provides direct *in situ* evidence in 3D for the dependence between the rate of heat-induced reshaping and the curvature of the branches of highly aniso-

Open Access Article. Published on 28 noiembrie 2018. Downloaded on 14.02.2026 15:02:16.
This article is licensed under a Creative Commons Attribution 3.0 Unported Licence.

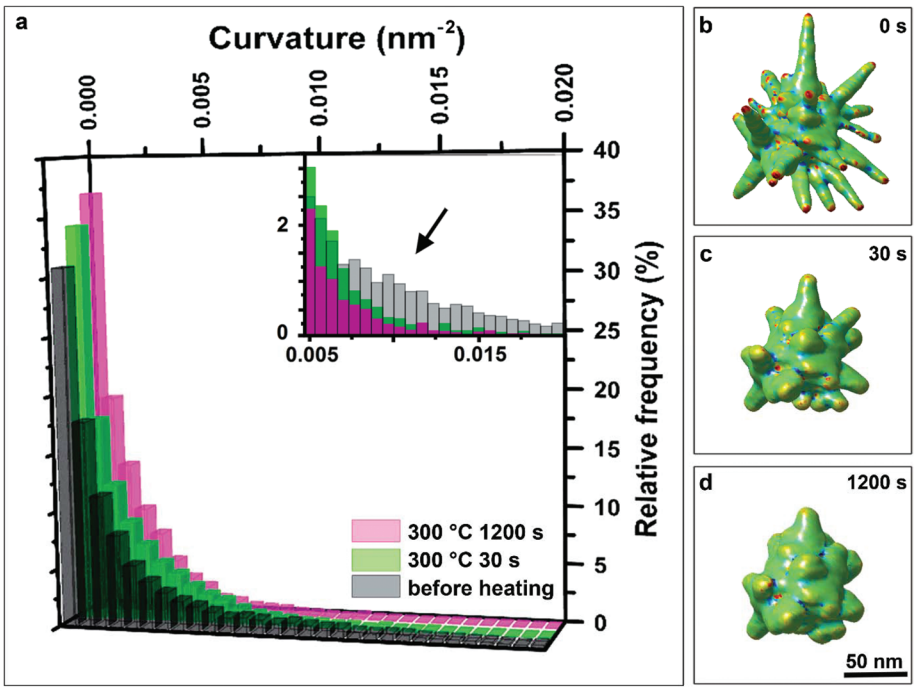

Fig. 5 (a) Histograms illustrating the measured curvature after different durations of heating at 300 °C. In every case, 30 bins were used to calculate the distribution. The inset illustrates a magnified 2D view of the histograms ranging from 0.005 nm^{-2} to 0.02 nm^{-2}, in which the black arrow highlights the loss of high curvature as function of temperature. Visualization of the curvature of the Au NS before heating (b), after 30 s of heating (c) and after 1200 s of heating (d). The color scale is directly related to the measured curvature values, red and blue representing high positive and high negative curvatures, respectively.

tropic NPs, which confirms the recently proposed curvature-induced surface diffusion mechanism for reshaping of Au NPs below the melting point.[16]

The decrease in curvature strongly alters the optical properties of the Au NS, which hampers applications where heating is involved. In order to evaluate the influence of the thermally induced morphological changes on the plasmonic properties of the Au NS, we performed BEM simulations using the MNPBEM toolbox.[39] Details on the simulations are provided in the ESI.† In short, the surface of the NSs were derived from their 3D tomographic reconstruction and discretized into 6000 vertices using Amira 5.4.0. The amount of vertices was chosen high enough to obtain a realistic depiction of the NSs' structure, while staying sufficiently low for computational considerations. The quasi-static approximation was employed to calculate the optical properties of the NSs as a function of temperature. Fig. 6a displays the extinction spectra calculated for the unheated and heated NS at 300 °C for 30 s and 1200 s. The polarization direction was chosen along the *x*-axis and the particle was rotated in order to align one tip with the polarization direction. Due to the complex structure of the NP, the spectra contain several peaks which was also observed in previous studies.[40,41] For the extinction spectrum of the unheated NS (black curve) the peak at 805 nm is attributed to the tip aligned with the *x*-axis (see Fig. S11†). Upon heating, it is obvious that the longitudinal LSPR peaks drastically blue-shifts due to the loss of sharpness of the tip and decrease in aspect ratio. Specifically, after 1200 s of heating at 300 °C, the maximum of the extinction cross section dropped by a factor of 10 and the resonance peak connected to the peak aligned along the *x*-axis shifts from 800 nm to 605 nm after 30 s and to 600 nm after 1200 s of heating (Fig. S9†).

The deformation of the tip also has a direct influence on the electric field amplification and in turn on the SERS enhancement. Therefore, we calculated the average electric field enhancement under illumination wavelength ranging from 500 nm to 1000 nm. The results for 300 °C are shown in Fig. 6b–d. As expected from the extinction cross sections, the electric field enhancement drops significantly upon heating. Specifically, the enhancement drops by 73% upon heating the NS for 30 s at 300 °C and continues to decrease by 82% of the original enhancement after heating for 1200 s. The extinction cross sections and the induced electric fields for the NSs heated at 200 °C and 400 °C are presented in Fig. S10 and S11.† Due to the less severe deformation of the NS heated at 200 °C, the changes in the extinction spectrum and the drop in field enhancement are not as drastic as for 300 °C, but still the field enhancement drops by 44% after heating for 30 s (Fig. S10b–d†). At 400 °C, almost all interesting plasmonic features are lost due to the strong deformation to a quasi-spherical shape (Fig. S11b–d†). As a result, for applications where elevated or even moderate temperatures are required, *e.g.* certain photocatalytic reactions, the observed decrease in field enhancement will influence their efficiency. Therefore, the

 This journal is © The Royal Society of Chemistry 2018

Open Access Article. Published on 28 noiembrie 2018. Downloaded on 14.02.2026 15:02:16.
This article is licensed under a Creative Commons Attribution 3.0 Unported Licence.

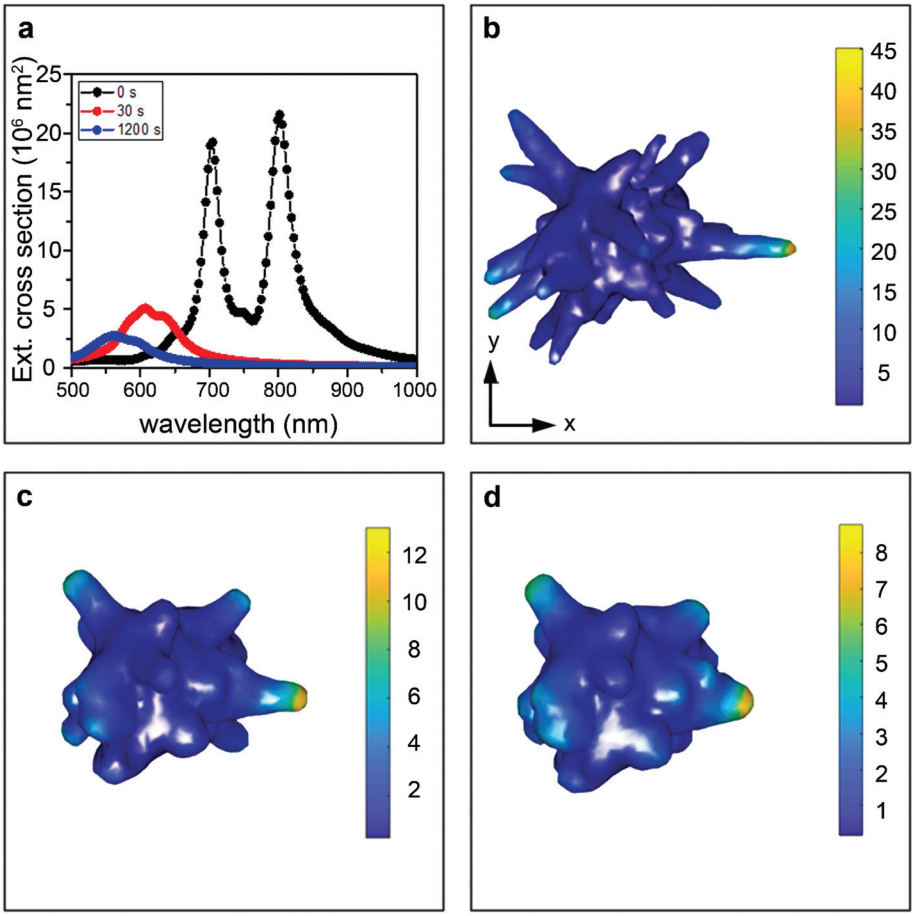

Fig. 6 BEM simulations of the Au NS heated at 300 °C, performed on a simplified surface deduced from the corresponding 3D tomographic reconstructions. (a) Extinction cross sections for the unheated and heated NS, after 30 s and 1200 s of heating at 300 °C. The calculated average induced electric field is shown for the unheated NS (b), after heating for 30 s at 300 °C (c) and after heating for 1200 s at 300 °C (d).

information that can be provided by our experiments is of crucial importance when incorporating these materials in future applications.

Conclusions

We implemented a novel methodology to perform fast electron tomography, which allowed us to observe the morphological evolution of Au NSs heated at 200 °C, 300 °C and 400 °C, at different time steps up to 1200 s. Due to the highly reduced acquisition time of the tilt series, gradual changes at distinct time steps during heating were investigated, which allowed us to record the 3D morphological changes as a function of heating time and temperature. We were thereby able to quantify local volume reductions and increments, as well as determine the local curvatures of NSs during heating. At elevated temperatures, the sharp tips at the end of the nanobranches were observed to reshape into shorter and blunter tips. While it has been previously postulated by indirect methods that curvature-induced surface diffusion is the driving mechanism of such reshaping, our experiments directly confirm this hypothesis. We additionally show that the major part of the morphological evolution occurs within the first minute of heating, regardless of temperature. The shape transition subsequently slows down and a stable final morphology is reached. The total amount of reshaping was found to increase for higher temperatures and the final morphology of the NSs to depend on the heating temperature, which thus has a more significant influence than the heating time. From BEM simulations we additionally showed that reshaping leads to a drastic decrease in electric field enhancement, which must be taken into account for applications where heating of NPs is unavoidable. It should be noted that the proposed procedure for fast HAADF-STEM tomography is general and not constrained to specific NP shapes or compositions. We expect that this approach will be essential to investigate other dynamical processes under different *in situ* conditions.

Conflicts of interest

There are no conflicts to declare.

Open Access Article. Published on 28 noiembrie 2018. Downloaded on 14.02.2026 15:02:16.
This article is licensed under a Creative Commons Attribution 3.0 Unported Licence.

Acknowledgements

H. V. acknowledges financial support by the Research Foundation Flanders (FWO grant 1S32617N). E. B. acknowledges a post-doctoral grant from the Research Foundation Flanders (FWO, Belgium). W. A. acknowledges an Individual Fellowship funded by the Marie Sklodowska-Curie Actions (MSCA) in Horizon 2020. The authors acknowledge funding from European Commission Grant (EUSMI 731019 to S. B., L. M. L.-M. and M. Z. and MUMMERING 765604 to S. B. and M. Z.). S.B. acknowledges financial support from European Research Council (ERC Starting Grant #335078-COLOURATOMS).

References

1 P. K. Jain, Gold Nanoparticles for Physics, Chemistry, and Biology. Edited by Catherine Louis and Olivier Pluchery, *Angew. Chem., Int. Ed.*, 2014, **53**(5), 395.
2 K. L. Kelly, E. Coronado, L. L. Zhao and G. C. Schatz, The optical properties of metal nanoparticles: The influence of size, shape, and dielectric environment, *J. Phys. Chem. B*, 2003, **107**(3), 668–677.
3 M. Pelton, J. Aizpurua and G. Bryant, Metal-nanoparticle plasmonics, *Laser Photonics Rev.*, 2008, **2**(3), 136–159.
4 C. F. C. Bohren and D. D. R. Huffman, *Absorption and Scattering of Light by Small Particles*, Wiley-VCH, 1998, vol. 98, pp. 544.
5 G. Baffou and R. Quidant, Thermo-plasmonics: Using metallic nanostructures as nano-sources of heat, *Laser Photonics Rev.*, 2013, **7**(2), 171–187.
6 J. Perez-Juste, I. Pastoriza-Santos, L. M. Liz-Marzan and P. Mulvaney, Gold nanorods: synthesis, characterization and applications, *Coord. Chem. Rev.*, 2005, **249**(17–18), 1870–1901.
7 N. Li, P. Zhao and D. Astruc, Anisotropic gold nanoparticles: synthesis, properties, applications, and toxicity, *Angew. Chem., Int. Ed.*, 2014, **53**(7), 1756–1789.
8 A. Espinosa, A. K. A. Silva, A. Sánchez-Iglesias, M. Grzelczak, C. Péchoux, K. Desboeufs, *et al.*, Cancer Cell Internalization of Gold Nanostars Impacts Their Photothermal Efficiency In Vitro and In Vivo: Toward a Plasmonic Thermal Fingerprint in Tumoral Environment, *Adv. Healthcare Mater.*, 2016, **5**(9), 1040–1048.
9 P. Senthil Kumar, I. Pastoriza-Santos, B. Rodríguez-González, F. Javier García De Abajo and L. M. Liz-Marzán, High-yield synthesis and optical response of gold nanostars, *Nanotechnology*, 2008, **19**(1), 015606.
10 A. Guerrero-Martínez, S. Barbosa, I. Pastoriza-Santos and L. M. Liz-Marzán, Nanostars shine bright for you. Colloidal synthesis, properties and applications of branched metallic nanoparticles, *Curr. Opin. Colloid Interface Sci.*, 2011, **16**(2), 118–127.
11 F. Hao, C. L. Nehl, J. H. Hafner and P. Nordlander, Plasmon resonances of a gold nanostar, *Nano Lett.*, 2007, **7**(3), 729–732.
12 J. Reguera, J. Langer, D. Jiménez de Aberasturi and L. M. Liz-Marzán, Anisotropic metal nanoparticles for surface enhanced Raman scattering, *Chem. Soc. Rev.*, 2017, **46**(13), 3866–3885.
13 M. L. Brongersma, N. J. Halas and P. Nordlander, Plasmon-induced hot carrier science and technology, *Nat. Nanotechnol.*, 2015, **10**, 25–34.
14 S. Mukherjee, F. Libisch, N. Large, O. Neumann, L. V. Brown, J. Cheng, *et al.*, Hot electrons do the impossible: Plasmon-induced dissociation of H2on Au, *Nano Lett.*, 2013, **13**(1), 240–247.
15 A. Manjavacas, J. G. Liu, V. Kulkarni and P. Nordlander, Plasmon-induced hot carriers in metallic nanoparticles, *ACS Nano*, 2014, **8**(8), 7630–7638.
16 A. B. Taylor, A. M. Siddiquee and J. W. M. Chon, Below melting point photothermal reshaping of single gold nanorods driven by surface diffusion, *ACS Nano*, 2014, **8**(12), 12071–12079.
17 S. Inasawa, M. Sugiyama and Y. Yamaguchi, Laser-induced shape transformation of gold nanoparticles below the melting point: The effect of surface melting, *J. Phys. Chem. B*, 2005, **109**(8), 3104–3111.
18 S. Link, C. Burda, B. Nikoobakht and M. A. El-Sayed, Laser-Induced Shape Changes of Colloidal Gold Nanorods Using Femtosecond and Nanosecond Laser Pulses, *J. Phys. Chem. B*, 2000, **104**(26), 6152–6163.
19 H. Petrova, J. Perez Juste, I. Pastoriza-Santos, G. V. Hartland, L. M. Liz-Marzán and P. Mulvaney, On the temperature stability of gold nanorods: comparison between thermal and ultrafast laser-induced heating, *Phys. Chem. Chem. Phys.*, 2006, **8**(7), 814–821.
20 G. Baffou, R. Quidant and C. Girard, Heat generation in plasmonic nanostructures: Influence of morphology, *Appl. Phys. Lett.*, 2009, **94**(15), 153109.
21 G. Baffou and H. Rigneault, Femtosecond-pulsed optical heating of gold nanoparticles, *Phys. Rev. B: Condens. Matter Mater. Phys.*, 2011, **84**(3), 035415.
22 L. Cao, D. N. Barsic, A. R. Guichard and M. L. Brongersma, Plasmon-Assisted Local Temperature Control to Pattern Individual Semiconductor Nanowires and Carbon Nanotubes, *Nano Lett.*, 2007, **7**(11), 3523–3527.
23 C. M. Tollan, R. Marcilla, J. A. Pomposo, J. Rodriguez, J. Aizpurua, J. Molina, *et al.*, Irreversible thermochromic behavior in gold and silver nanorod/polymeric ionic liquid nanocomposite films, *ACS Appl. Mater. Interfaces*, 2009, **1**(2), 348–352.
24 Y. Liu, E. N. Mills and R. J. Composto, Tuning optical properties of gold nanorods in polymer films through thermal reshaping, *J. Mater. Chem.*, 2009, **19**(18), 2704.
25 A. V. Whitney, J. W. Elam, P. C. Stair and R. P. Van Duyne, Toward a thermally robust operando surface-enhanced raman spectroscopy substrate, *J. Phys. Chem. C*, 2007, **111**(45), 16827–16832.
26 Y. Khalavka, C. Ohm, L. Sun, F. Banhart and C. Sonnichsen, Enhanced Thermal Stability of Gold and

 This journal is © The Royal Society of Chemistry 2018

Open Access Article. Published on 28 noiembrie 2018. Downloaded on 14.02.2026 15:02:16.
This article is licensed under a Creative Commons Attribution 3.0 Unported Licence.

Silver Nanorods by Thin Surface Layers, *J. Phys. Chem. C*, 2007, **111**(35), 12886–12889.

27 R. A. Crowther, D. J. DeRosier and A. Klug, The Reconstruction of a Three-Dimensional Structure from Projections and its Application to Electron Microscopy, *Proc. R. Soc. London, Ser. A*, 1970, **317**(1530), 319–340.

28 L. Roiban, S. Li, M. Aouine, A. Tuel, D. Farrusseng and T. Epicier, Fast "Operando" electron nanotomography, *J. Microsc.*, 2018, **269**(2), 117–126.

29 S. Nagashima, K. Ito, T. Aoki and H. Ishii, A High-Accuracy Rotation Estimation Algorithm Based on 1D Phase-Only Correlation, *Image Anal. Recognit. (Lecture Notes Comput Sci.)*, 2007, **4633**, 210–221.

30 H. Foroosh, J. B. Zerubia and M. Berthod, Extension of phase correlation to subpixel registration, *IEEE Trans. Image Process.*, 2002, **11**(3), 188–199.

31 K. Takita, T. Aoki, Y. Sasaki, T. Higuchi and K. Kobayashi, High-Accuracy Subpixel Image Registration Based on Phase-Only Correlation, *IEICE Trans. Fundam. Electron. Comput. Sci.*, 2003, **A86**(8), 1925–1934.

32 H. Yan and J.-G. Liu, Robust Phase Correlation based Motion Estimation and Its Applications, *Proc. Br. Mach. Vis. Conf.*, 2008, **2008**, 104.1–104.10.

33 W. J. Palenstijn, K. J. Batenburg and J. Sijbers, The ASTRA Tomography Toolbox: A platform for advanced algorithm development in electron tomography, *Ultramicroscopy*, 2015, **175**, 35–47.

34 T. K. Moon, The expectation-maximization algorithm, *IEEE Signal Proc. Mag.*, 1996, **13**(6), 47–60.

35 W. Albrecht, A. van de Glind, H. Yoshida, Y. Isozaki, A. Imhof, A. van Blaaderen, *et al.*, Impact of the electron beam on the thermal stability of gold nanorods studied by environmental transmission electron microscopy, *Ultramicroscopy*, 2018, **193**, 97–103.

36 B. Goris, M. A. Huis, S. Bals, H. W. Zandbergen, L. Manna and G. Van Tendeloo, Thermally induced structural and morphological changes of CdSe/CdS octapods, *Small*, 2012, **8**(6), 937–942.

37 N. Tian, Z.-Y. Zhou, S.-G. Sun, L. Cui, B. Ren and Z.-Q. Tian, Electrochemical preparation of platinum nanothorn assemblies with high surface enhanced Raman scattering activity, *Chem. Commun.*, 2006, (39), 4090–4092.

38 S. Rusinkiewicz, Estimating curvatures and their derivatives on triangle meshes, *Proceedings – 2nd International Symposium on 3D Data Processing, Visualization, and Transmission 3DPVT 2004*, 2004, 486–93.

39 U. Hohenester and A. Trügler, MNPBEM - A Matlab toolbox for the simulation of plasmonic nanoparticles, *Comput. Phys. Commun.*, 2012, **183**(2), 370–381.

40 C. L. Nehl, H. Liao and J. H. Hafner, Optical properties of star-shaped gold nanoparticles, *Nano Lett.*, 2006, **6**(4), 683–688.

41 T. V. Tsoulos, L. Han, J. Weir, H. L. Xin and L. A. Fabris, Closer Look at the Physical and Optical Properties of Gold Nanostars: An Experimental and Computational Study, *Nanoscale*, 2017, **9**(11), 3766–3773.